AD-A115 693 MARTIN MARIETTA LABS BALTIMORE MD F/G 11/6
THE DELAYED FRACTURE OF ALUMINUM ALLOYS, END OF YEAR REPORT,(U)
MAR 82 J R PICKENS, D VENABLES, G D DAVIS N00014-81-C-0342
UNCLASSIFIED MML-TR-82-9C NL

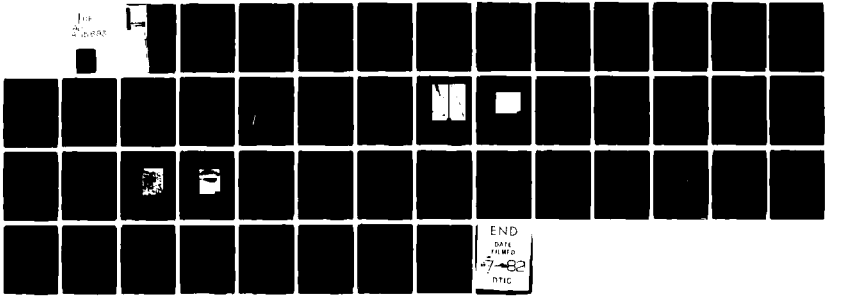

(3)

MML TR 82-9(c)

THE DELAYED FRACTURE OF ALUMINUM ALLOYS

End of Year Report

March 1982

Prepared by:
J.R. Pickens, D. Venables, G.D. Davis,
and J.R. Gordon
MARTIN MARIETTA CORPORATION
Martin Marietta Laboratories
1450 South Rolling Road
Baltimore, MD 21227-3898

Prepared for Contract N00014-81-C-0342
Office of Naval Research
Department of the Navy
800 North Quincy Street
Arlington, Virginia 22217

Distribution of This Document is
Unlimited.

Unclassified

SECURITY CLASSIFICATION OF THIS PAGE (When Data Entered)

REPORT DOCUMENTATION PAGE		READ INSTRUCTIONS BEFORE COMPLETING FORM
1. REPORT NUMBER MML TR 82-9 (c)	2. GOVT ACCESSION NO. AD-A115693	3. RECIPIENT'S CATALOG NUMBER
4. TITLE (and Subtitle) The Delayed Fracture of Aluminum Alloys End of Year Report		5. TYPE OF REPORT & PERIOD COVERED End of Year Report 3/16/81 - 3/15/82
		6. PERFORMING ORG. REPORT NUMBER MML TR 82-9(c)
7. AUTHOR(s) Joseph R. Pickens, David Venables Guy D. Davis, Jonathan R. Gordon		8. CONTRACT OR GRANT NUMBER(s) N00014-81-C-0342
9. PERFORMING ORGANIZATION NAME AND ADDRESS Martin Marietta Corporation Martin Marietta Laboratories 1450 South Rolling Road, Baltimore, MD 21227-3898		10. PROGRAM ELEMENT, PROJECT, TASK AREA & WORK UNIT NUMBERS
11. CONTROLLING OFFICE NAME AND ADDRESS Department of the Navy Office of Naval Research, Code 471 800 North Quincy Street, Arlington, VA 22217		12. REPORT DATE March 1982 13. NUMBER OF PAGES 47
14. MONITORING AGENCY NAME & ADDRESS(if different from Controlling Office)		15. SECURITY CLASS. (of this report) Unclassified 15a. DECLASSIFICATION/DOWNGRADING SCHEDULE

16. DISTRIBUTION STATEMENT (of this Report)

Distribution of this document is unlimited

17. DISTRIBUTION STATEMENT (of the abstract entered in Block 20, if different from Report)

18. SUPPLEMENTARY NOTES

19. KEY WORDS (Continue on reverse side if necessary and identify by block number)

Aluminum alloys, stress corrosion cracking, oxide film, Auger electron spectroscopy, Mode I, Mode III, Hydrogen embrittlement, constituent particles, plasmon loss energy, grain boundary segregation

20. ABSTRACT (Continue on reverse side if necessary and identify by block number)

The mechanisms of failure of high-strength aluminum alloys in saline environments was investigated. It was found that the mechanism of stress corrosion cracking (SCC) in a commercial Al-Mg alloy, 5083, is dominated by hydrogen embrittlement (HE). The dominant contribution of HE was discerned by comparing SCC susceptibility under Modes I and III loading.

The influence of the surface oxide film on the SCC susceptibility of 7075 and 7175 alloys was also examined. It was found that unlike certain high-

DD FORM 1 JAN 73 1473

Unclassified

SECURITY CLASSIFICATION OF THIS PAGE (When Data Entered)

20. (cont.)

purity alloys, the susceptibility of these commercial alloys is not significantly influenced by the composition of the oxide. In these 7xxx alloys, the insoluble constituent particles provide sites for SCC initiation. The greater susceptibility of 7075, compared with its higher purity version, 7175, is in part a result of its lower value fraction of the constituent particles.

Attempts by micro-micro diffraction and plasmon energy loss measurements failed to establish the existence of a Mg-H or Al-H complex. Its existence remains speculative.

Slight changes in solution heat treatment temperature (SHT) were found to significantly alter the susceptibility of Al-Zn-Mg alloys. The influence of SHT appears to be related to solute segregation to grain boundaries and grain boundary microstructure, but not to oxide film composition.

FOREWORD

This report presents the results of work performed at Martin Marietta Laboratories from 15 March 1981 to 1 February 1982 for the Office of Naval Research, Contract No. N00014-81-C-0342.

TABLE OF CONTENTS

I. BACKGROUND

Mechanistic studies at Martin Marietta Laboratories of the stress-corrosion cracking (SCC) of Al-Zn-Mg alloys have proceeded through several stages of emphasis. For example, early research concentrated on the dissolution mechanism of cracking.[1-3] Subsequent studies assessed the role of hydrogen embrittlement (HE) in SCC,[4-5] while more recent research has investigated the role of segregation phenomena in cracking.[6-11] Some of our major contributions to the understanding of SCC of Al-Zn-Mg alloys include: that SCC resistance increases with increasing spacing of precipitates at the grain boundary;[1] HE constitutes the major contribution to cracking (as found by examining the effect of loading mode on SCC resistance;[5] and magnesium segregates to the regions involved in SCC — the surface oxide film[6,7] and the grain boundary.[8-11] This last finding, i.e., that Mg is present both in the grain boundary and the surface oxide film, led us to propose a mechanism of cracking by which Mg and H interact to form a Mg-H complex.[11] This interaction would enable hydrogen atoms, released in the cathodic half of the dissolution reaction, to be captured and to remain in the alloy rather than form H_2 gas. Moreover, it has been hypothesized[11] that the significant amount of unbound Mg found segregated to the grain boundary facilitates hydrogen concentration on the grain boundary.

Over the last several years, we have endeavored to demonstrate the negative effect of Mg on SCC resistance. For example, we have shown that for a constant solute content (wt%Zn plus wt%Mg), SCC resistance decreases with the ratio of bulk Zn to Mg in weight percent (Zn/Mg hereafter) for $1.2 \leq Zn/Mg \leq 2.9$.[12,13] In addition, we found that the Mg-enriched "thermal" film that forms during solution heat treatment[7] provides substantially less SCC protection than an alumina film of equivalent thickness.[12,14,15] Moreover, the extent of the Mg segregation in the film is a sensitive function of the solution heat-treatment temperatures (SHT) examined.[7]

During the past year, we evaluated the possibility that SCC in Al-Mg alloys (i.e., Zn-free) also involves HE, through investigations of the effect of loading mode on the SCC susceptibility of commercial 5083. We also expanded our work showing that a Mg-rich thermal film provides less SCC resistance than a Mg-free film for commercial 7xxx alloys. This latter work was undertaken to further elucidate the effect of film composition on SCC initiation and to determine if control of film composition has the potential to provide a means of commercially decreasing SCC susceptibility. We also sought to provide evidence for the existence of the suspected Mg-H complex by micro-micro diffraction and by plasmon-loss energy measurements. Finally, we systematically varied SHT to determine its effects on SCC resistance. We then characterized grain boundary and oxide film compositions by Auger electron spectroscopy (AES) to explain any changes in SCC resistance.

The experimental procedures and results of these studies are described in the following sections.

II. RESULTS IN 1981

A. THE EFFECT OF LOADING MODE ON THE SCC SUSCEPTIBILITY OF Al-Mg ALLOY 5083

1. Background

Green et al.,[4,5] reported an experiment for determining whether HE is involved in the SCC mechanism for a given alloy. They compared the time to failure (ttf) in SCC environments in Mode I (tension) and Mode III (antiplane shear, i.e., torsion), and concluded that differences in ttf at a given normalized stress intensity provide evidence that HE is operating, as rationalized below. In Mode I, a triaxial tensile stress field exists ahead of a crack tip[16] and dissolved (atomic) hydrogen is known to collect at such regions of triaxiality.[17] This process provides a driving force for hydrogen to concentrate sufficiently for embrittlement. On the other hand, no such triaxial region exists in Mode III, so there is no driving force for hydrogen collection and subsequent embrittlement, even in alloys that are extremely susceptible to HE. Green et al.[4,5] reason that the behavior of an alloy to this difference in triaxiality can be used as a diagnostic tool to determine if cracking under load in a corrosive environment involves HE, or is primarily attributable to dissolution.

They demonstrated the validity of the test method by loading specimens of Ti-8wt%Al-1wt%Mo-1wt%V alloy in a saline environment at various normalized stress intensity levels -- K_I/K_{IC} and K_{III}/K_{IIIC} — and measuring ttf.[4] SCC in this alloy is known to involve HE, and the plot of normalized stress intensity vs ttf for Mode I reveals much greater susceptibility (lower ttf) than the plot for Mode III.[4] They then examined[5] alpha-brass in aqueous ammonia because the cracking mechanism in this SCC system is believed not to involve HE.[18] The normalized

stress intensity vs ttf curves roughly coincided for the two loading modes as the investigators predicted.[5] This important result showed that the corrosive solution had access to the crack tip in each mode.

Since the test method was shown to be valid by the titanium and brass experiments, Green et al.[5] examined aluminum alloy 7075 in a saline environment. As with the titanium alloy, ttf in Mode I was much less than in Mode III at a given normalized stress intensity level. They then added As, a known hydrogen recombination inhibitor,[19] and observed increased embrittlement in Mode I and reduced embrittlement in Mode III. The rationale given for this latter result was as follows. Under Mode I loading, where hydrostatic stresses force hydrogen to a region of triaxial stress ahead of the crack tip, the addition of arsenic retards the kinetics of hydrogen evolution, thereby increasing hydrogen concentration within the metal, which enhances the hydrogen embrittlement. Under Mode III loading, however, there is insufficient hydrostatic stress to cause the localized concentration of hydrogen; thus, the slower dissolution mechanism takes precedence. In this experiment, the arsenic served to retard the cathodic reaction, $2H^+ + 2e^- \rightarrow H_2$, which controls the rate of the overall dissolution process. Thus, they concluded that the SCC mechanism in 7075 involves HE.

It is known that the Al-Mg (5xxx) alloys are susceptible to SCC if the Mg content is slightly higher than the room-temperature solubility limit (~ 3 wt%) and if a substantial amount of the β phase, Mg_2Al_3, has precipitated on the grain boundaries.[20] The β-phase precipitation is stimulated by cold work,[20] and to a greater extent by exposure to elevated temperatures. Susceptibility typically increases with the continuity of the β-phase layer.[20] Mg_2Al_3 is strongly anodic with respect to the Al-Mg solid-solution matrix and dissolves rapidly in saline environments. Hence, the mechanism of SCC in Al-Mg alloys generally has been accepted to proceed by dissolution of the β phase.

In the present study, we investigated the role of HE in the SCC mechanism in a commercial Al-Mg alloy by performing the previously

described loading mode experiment on alloy 5083. The mechanics of the experiment were improved over the earlier procedures.[5] Results are discussed with respect to the role of Mg in the cracking process.

2. Materials

We used a high-strength Al-Mg alloy to maintain the specimens at a size small enough to be practical, yet large enough to satisfy minimum size requirements for linear elastic-fracture mechanics. High-strength Al-Mg alloys, which are not age hardenable, are often strengthened by cold working during rolling. Commercial material that met size and strength requirements was from 3.81-cm-thick armour plate of 5083 H131, available from Martin Marietta Aluminum's rolling plant in Lewisport, Kentucky. We did not use a model, high-purity Al-Mg alloy in the present work because ingot and specimen sizes would have been too large to be practical.

We sensitized the 5083 by exposure to 150°C for 72 hours. This sensitization resulted in a minor loss in ultimate tensile strength, but a substantial drop in yield strength (see Table I). Alloy composition is shown in Table II. The mean linear-intercept grain size was 275 μm in the short-transverse direction.

The following stress-corrosion environment, evaluated previously by Sprowls et al.,[21] was used:

$$0.6\ M\ (3.5\ wt\%)NaCl + 0.02\ M\ Na_2Cr_2O_7 + 0.07\ M\ NaC_2H_3O_2 + HC_2H_3O_2;\quad pH = 4.$$

This solution inhibits general corrosion and accurately simulates SCC in seawater.[22]

TABLE I

Long-Transverse Tensile Properties of 5083

Temper	0.2% Yield Strength (ksi)	Ultimate Tensile Strength (ksi)	K_{IC} (MPa $\sqrt{m}$)
H131	41.0	50.8	24.2
Sensitized	29.0	46.0	33.4

TABLE II

Composition (wt%) of 5083

Mg	Mn	Cr	Fe	Si	Ti	Cu	Zn	Al
4.4	0.70	0.13	0.29	0.16	0.021	< 0.2	< 0.2	Balance

3. Experimental Procedure

a. Mode I Specimens

We selected the compact tension (CT) specimen geometry in the T-L[23] orientation for this work (see Fig. 1). After sensitization, the properties of the specimen did not satisfy the conservative Brown and Strawley[24] criterion: $B \geq 2.5(K_{IC}/YS)^2$ where B = minimum specimen width and YS = yield strength (English units). Using K_{IC} = 30 ksi $\sqrt{in.}$ and the measured YS, we obtained B = 6.86 cm, which is greater than the 3.81-cm specimen width. However, our specimen size was made as large as possible given the size of the plate.

All Mode I specimens contained a fatigue precrack introduced at K_{Imax} = 16 ksi $\sqrt{in.}$ at 20 cycles per second, and we measured K_{IC} on two specimens to select stress intensity levels for SCC testing.

We performed a compliance calibration and stressed the specimens under constant load in an MTS servo-hydraulic test system with a 10,000-lb capacity. The specimens were subjected to "alternate immersion" (10 min wet and 50 min dry) in the test solution. The displacement of the loading pins was measured and plotted as a function of time. This information, along with the compliance calibration, enabled us to generate curves of crack velocity vs stress intensity.

b. Mode III Specimens

For Mode III, we used a torsion apparatus similar to that used by Green et al.,[5] but modified their cylindrical specimen configuration by sharpening the notch (Fig. 1); we introduced fatigue precracking by imposing a constant bending moment on each notched specimen in a lathe for 15 min at 120 rpm. To estimate the initial precrack size after fracture, we measured the area of the initial test ligament using a Hewlett-Packard digitizer, found the radius of a circle having the same area, and subtracted the value of this radius from the size of the test

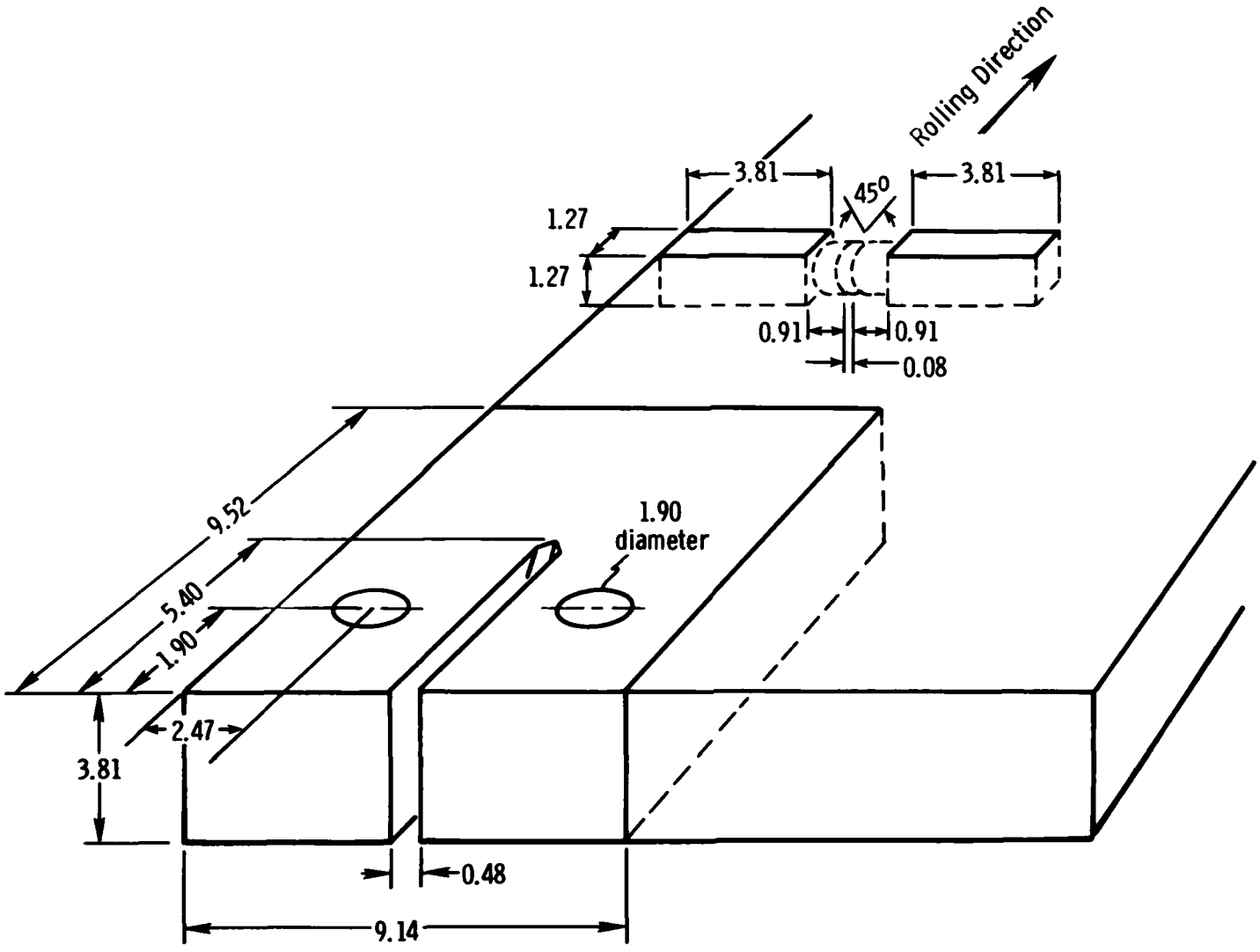

Figure 1. Orientation of compact tension (Mode I) and torsion (Mode III) specimens from 5083 plate. (dimensions in cm)

ligament before precracking. This method enabled us to account for the irregularity of several crack fronts.

We placed specimens under constant load and under alternate immersion in the stress-corrosion environment used in the Mode I tests.

4. Results

Measurements of the critical stress intensities in each mode are necessary to normalize the stress intensity levels so that they can be meaningfully compared. We computed K_{IC} to be 30.4 ksi $\sqrt{in.}$ using the following equation for K_I:

$$K_I = (P/BW^{1/2}) \cdot \frac{(2 + a/W)(0.886 + 4.64a/W - 13.32a^2/W^2 + 14.72a^3/W^3 - 5.6a^4/W^4)}{(1 - a/W)^{3/2}}$$

where P = load in lb_f

B = thickness of specimen in inches

W = width of specimen in inches

a = crack length

as described in ASTM E399.[23]

We computed K_{IIIC} to be 11.0 ksi $\sqrt{in.}$ using the following equation for K_{III}:[25]

$$K_{III} = \frac{2T}{\pi a^3} \sqrt{\pi a} \left[\frac{3}{8} \left(1 + \frac{1}{2} \left(\frac{a}{b}\right) + \frac{3}{8} \left(\frac{a}{b}\right)^2 + \frac{5}{16} \left(\frac{a}{b}\right)^3 + \frac{35}{128} \left(\frac{a}{b}\right)^4 + 0.208 \left(\frac{a}{b}\right)^5 \right) \right]$$

$$\cdot \left(\sqrt{1 - a/b} \right)$$

where T = torque

b = 1/2 the ligament diameter.

We obtained a different value for K_{IIIC} using an alternative equation.[26] Figure 2 gives the compliance curves in Mode I.

With accurate values of K_{IC} and precise (although possibly not accurate) values of K_{IIIC}, the SCC data in each mode can be compared. Figure 3, a plot of K_I/K_{IC} and K_{III}/K_{IIIC} vs ttf, reveals a much longer life in Mode III than in Mode I. In fact, at $K_{III}/K_{IIIC} = 0.9$, a Mode III specimen did not fail in 1,500 hours. As shown in Fig. 3, the addition of arsenic to the SCC environment substantially decreased ttf in Mode I.

The crack velocity (υ) curve, log υ vs log K_I, reveals a plateau velocity of 2×10^{-2} mm/hour (Fig. 4), but the SCC threshold was not obtained.* The stress-corrosion crack velocity in Mode III could not be accurately measured but appears to be an order of magnitude less than that in Mode I, based on the observed crack advance preceding failure and the elapsed time.

The sensitization treatment was successful in producing a semi-continuous layer of Mg_2Al_3 on the grain boundaries (Fig. 5) and annihilated a significant amount of substructure. The SCC fracture path was largely intergranular (Fig. 6).

5. Discussion

To our knowledge, K_{IIIC} for 5083 has not been reported in the literature; nevertheless, it was surprising to learn that K_{IIIC} is substantially less than K_{IC}. We computed K_{IIIC} using an alternative equation[26] and obtained an even lower result. If the values of K_{III} and K_{IIIC} are not accurate, the ratio K_{III}/K_{IIIC} should be reasonably accurate because the load is known with excellent accuracy and the precrack length did not vary significantly from specimen to specimen. Consequently, comparison of K_{III}/K_{IIIC} with K_I/K_{IC} is reasonable regardless of the accuracy of K_{IIIC}. The fractures in Mode I were fairly flat, suggesting that plane strain conditions were largely maintained.

* When using double cantilever beam specimens under constant load, K_I decreases with crack advance so the SCC threshold (K_{ISCC}) can be accurately measured when the crack arrests. In contrast, for CT specimens, K_I increases with crack advance, and the test begins at $K_I > K_{ISCC}$, which precludes K_{ISCC} measurement.

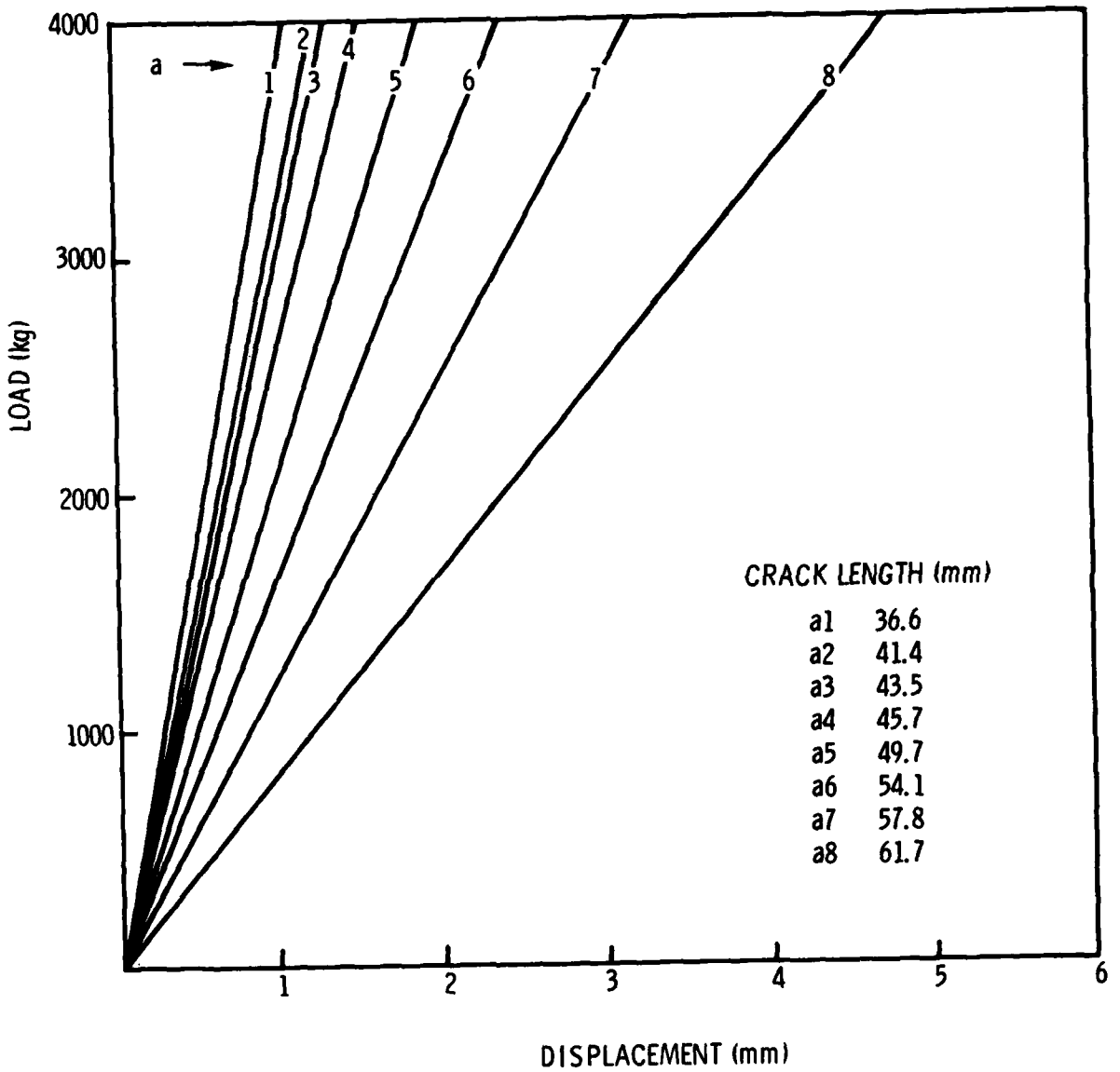

Figure 2. Load displacement curves from which compliance calibration was made.

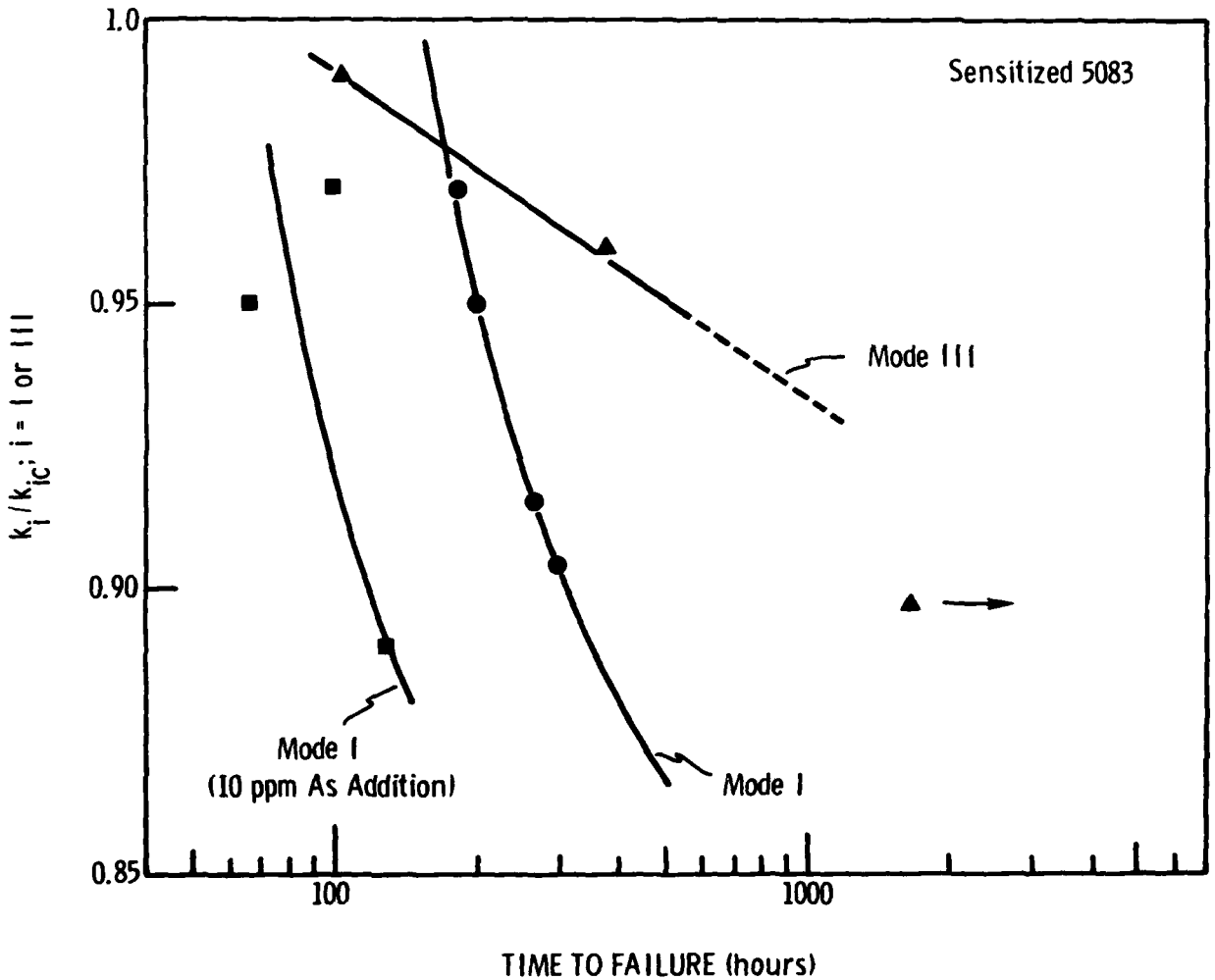

Figure 3. Effect of loading mode on time to failure in salt-dichromate-acetate solution (alternate immersion) for sensitized 5083.

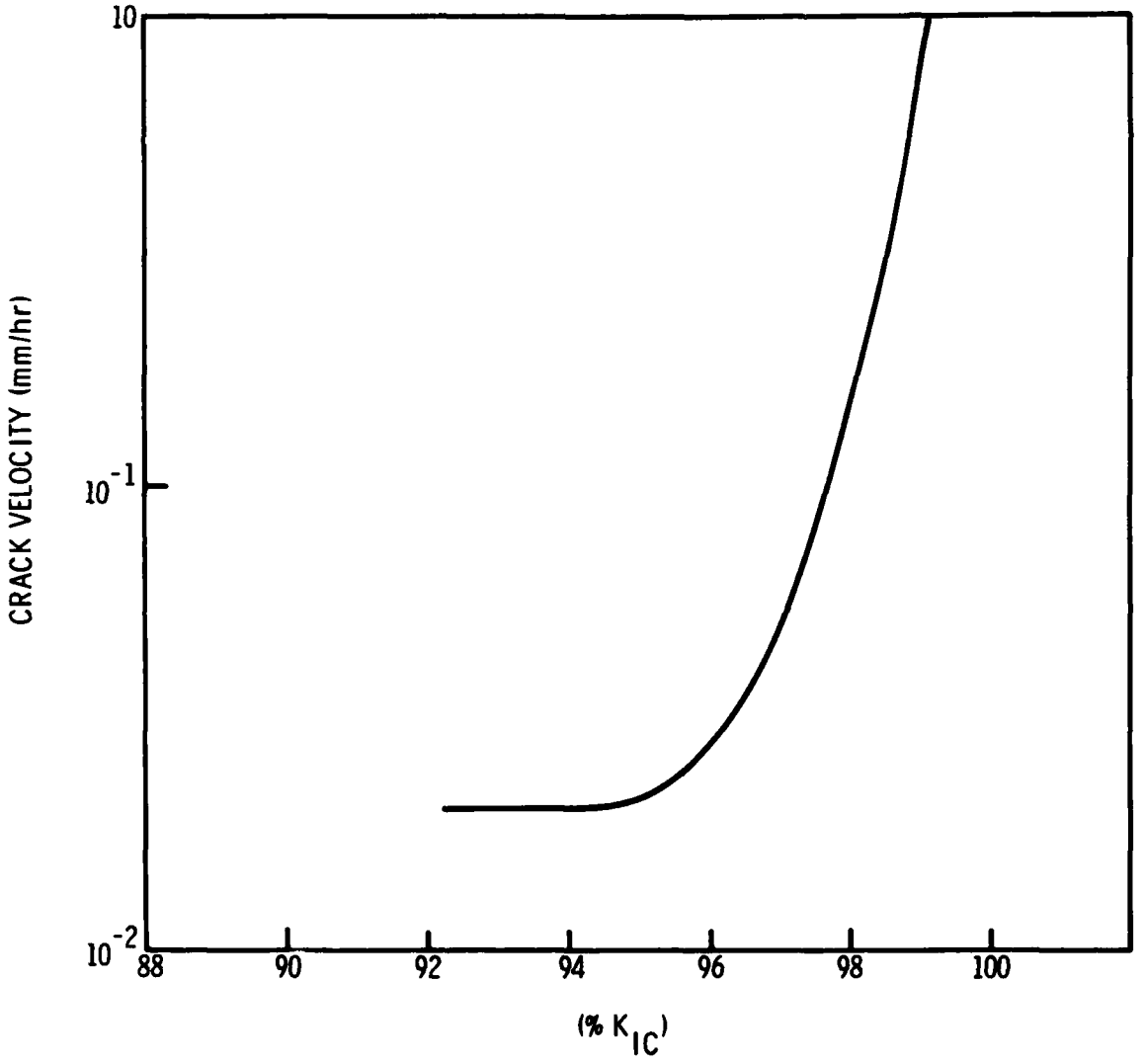

Figure 4. Crack velocity vs K_I curve for sensitized 5083.

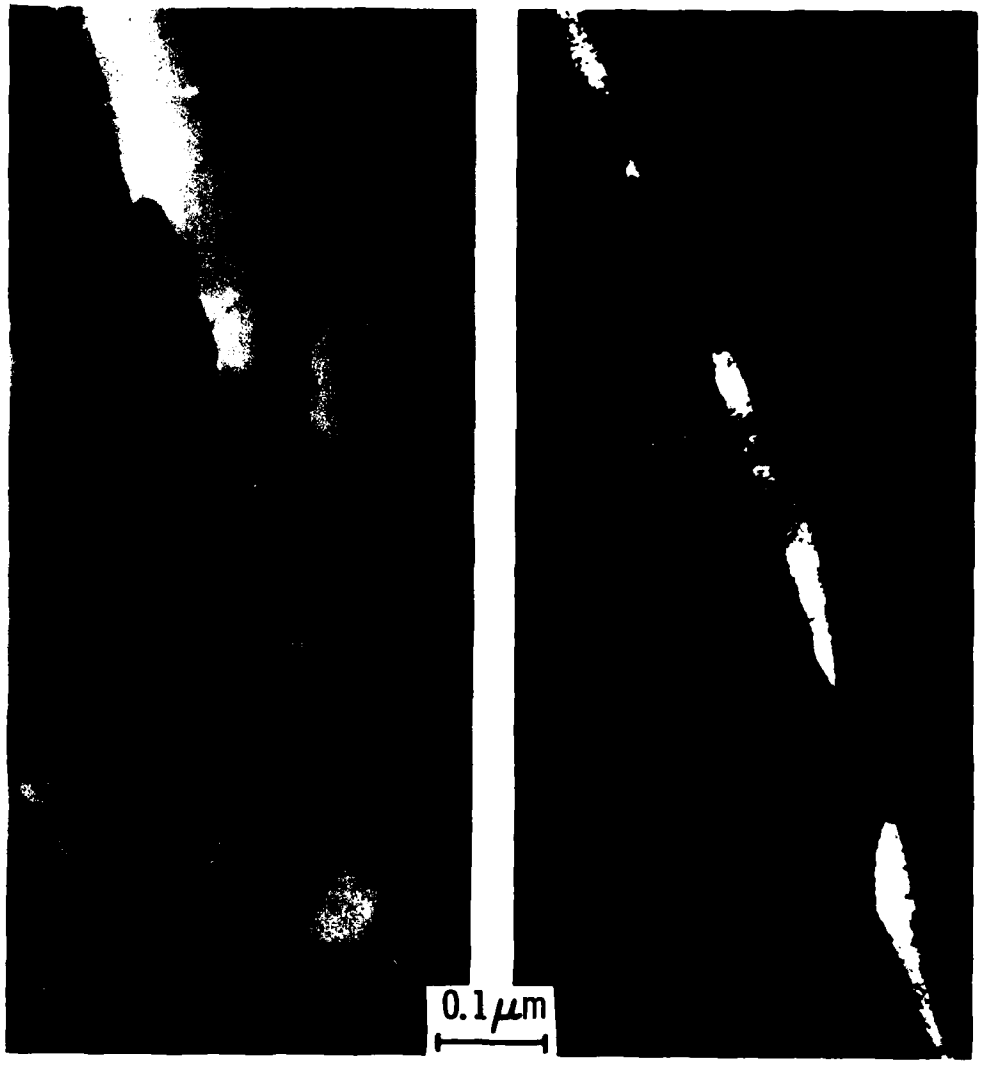

Figure 5. β phase decorating grain boundaries in sensitized 5083 aluminum alloy.

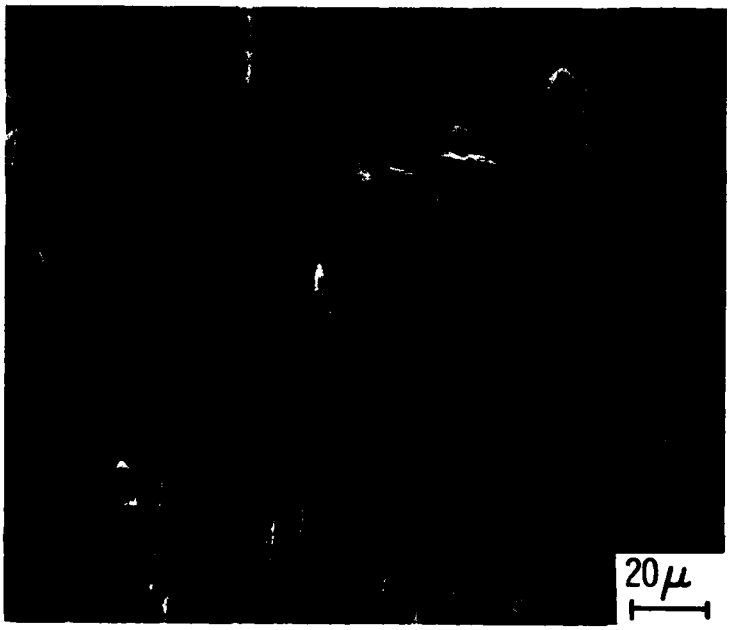

Figure 6. Mode I fracture surface of sensitized 5083 showing intergranular SCC.

To establish whether HE is a factor in the SCC of a 5xxx alloy, the major purpose of this study, we compared loading in Modes I and III and found a substantial difference in ttf at a given normalized stress intensity (ttf in Mode III ~ 5 times ttf in Mode III). Furthermore, the decrease in ttf in Mode I in the presence of As provides additional strong evidence that the SCC mechanism involves HE. Since some Mode III specimens, even without As, endured 1,500 hours without failure, we did not consider it practical to add As to the solution in Mode III.

The above observations strongly indicate that HE contributes significantly to stress-corrosion cracking in 5083. That is, the farther the Mode I curve is displaced to the left of the Mode III curve (see Fig. 3), and the farther the additional displacement of the Mode I curve in the presence of As, the greater the contribution of HE.

Recent work by Japanese researchers[27-30] has shown that an Al-8wt%Mg alloy is susceptible to pre-exposure embrittlement, which is a type of HE. Their result, albeit on an alloy containing higher Mg, is consistent with ours.

It is interesting to consider which aspects of the composition and microstructure enable the HE mechanism to operate. Early investigators speculated that in 7xxx Al-Zn-Mg alloys, HE was related to the Zn content, and alloys not containing Zn might be immune to cracking.[31] Recent work by Auger electron spectroscopy has identified Mg on grain boundaries[8-11] that is not bound in precipitates and Mg segregation in the surface oxide film[6,7] of Al-Zn-Mg alloys that are susceptible to SCC. In contrast, virtually all grain-boundary Zn is bound in $MgZn_2$ precipitates,[8-11] and Zn was not found to segregate to the surface oxide film. This result led to the proposal that HE occurs by a mechanism involving the formation of a Mg-H complex.[11] The susceptibility to cracking of 5083, a Zn-free alloy, is consistent with this model. In our future work, we plan to determine if free Mg segregates to the grain boundaries in 5083.

Several criticisms of the loading mode technique used in the earlier work have been raised. For example, some suggested that the

corrosive solution did not have equal access to the crack tips in each loading mode. In rebuttal, Green et al.[5] claim that in both loading modes, the surface oxide as well as atomic bonds are strained so that the corrosive solution presumably has similar access to the metal substrate. Further, their experiment on α-brass corroborates this view.

Others questioned whether pure Mode III loading could be attained, i.e., whether there was not a component of Mode I (whether macroscopic or around microstructural heterogeneities) accompanying the torsional loading? This certainly is possible, but a superimposed Mode I component would tend to <u>decrease</u> ttf in Mode III, and bring the Mode I and Mode III curves together. Thus, in the case where HE is shown to be operating in the alloy, any component of Mode I on the Mode III specimens would tend to obscure the evidence that HE is operating, but this effect would not refute the validity of the method. One could legitimately argue that HE could be operative when the normalized stress intensity vs ttf curves roughly coincided because an unwanted Mode I component could exist in the Mode III test. The shift of the Mode I vs ttf curves under the influence of arsenic can be used as a means of illuminating this point. That is, if the Mode I curve shifts to the left in the presence of As -- shorter ttf in Mode I -- then HE is operating in the SCC process in Mode I. If there is no shift, HE is not operating.

We can also identify three additional areas of concern for the validity of the loading mode comparison:

1) <u>Differences in mechanical locking of opposing SCC surfaces</u>. A SCC path often winds circuitously around grains and inclusions. Such a path could lead to mechanical interlocking in Mode III where the opposing crack planes slide over each other. This locking is not likely in Mode I where the two opposing crack surfaces tend to be pulled apart. While it might occur in Mode III, its effect is considered minor in our experiment on 5083. Also, such an effect could not account for the influence of As in the test solution on the ttf curves shown by Green and Hayden. [4]

2) Effect on specimen size. A substantial fraction of the ttf in Mode I is spent in the "plateau region"[32] where crack velocity is independent of K_I. Therefore, the ttf could be increased by making the Mode I specimens larger. Furthermore, there is no requirement for a standard specimen size in Mode III, nor is there a well-established analytical procedure to suggest relative sizes of the two specimen types. In the present work, we made the Mode I specimens larger than the Mode III specimens so that ttf in Mode I would be "rather long" compared with that in Mode III. Thus, the much longer ttf in Mode III than in Mode I (ttf ~ 5 times longer) further supports the view that HE is involved in the SCC mechanism.

3) Differences in the deformation zone. The dimensions of the deformation zones in Mode I and Mode III are quite different. Broek[33] compared analytical estimates of the plastic zone geometries in the two modes and showed numerous differences, the most interesting of which are in the plastic zone "radius" directly ahead of the crack tip. This difference would probably result in variations in hydrogen transport by dislocations in the two modes. This interesting area deserves further study.

6. Implications of Current Findings

HE may be partly responsible for cracking during industrial processing of high-magnesium 5xxx alloys. For example, the mechanism of edge cracking in 5xxx sheet and plate may partly result from hydrogen introduced during casting or hot rolling in the presence of moisture. Recently, Thomson and Burman[34] found that edge cracking in 5xxx alloys was greater in alloys containing more than 0.04 ml hydrogen per 100 g alloy. They also proposed that a sodium-hydrogen synergism leads to increased edge cracking.

In addition, pickup of hydrogen during welding of 5xxx alloys may also lead to embrittlement. Welding procedures currently guard against hydrogen pickup, and our current findings underscore the importance of this practice.

B. REDUCING SCC SUSCEPTIBILITY OF COMMERCIAL 7xxx ALLOYS BY CONTROLLING OXIDE FILMS

1. Background

In our earlier work, we found that the SCC susceptibility of a high-purity, fine-grained Al-4.4wt%Zn-3.7wt%Mg alloy could be reduced by using caustic etching (CE) to remove the Mg-rich "thermal" film formed during solution heat treatment. After CE, a Mg-free "natural film forms." [12] We also found that the thermal film on a coarse-grained Al-4.4wt%Zn-3.7wt%Mg alloy provided significantly less SCC protection than an alumina film of equivalent thickness formed by anodizing in tartaric acid.[14,15] In the past year, we extended this work to commercial 7xxx alloys to try to reduce SCC susceptibility in these more complex materials.

2. Experimental Procedure

Short-transverse tensile samples, 1.5 x 0.25 x 0.50 in. with a 0.75-in. test section, were machined from extruded bars of 7075 and 7175 alloys (compositions in Table III). Each alloy had an elongated grain structure measuring ~ 170 x 20 x 20 μm. We polished the specimens to a 600-grit finish and re-heat treated them to the T6 temper as follows: heating at 475°C for 2 hours, ice water quench, heating at 121°C for 24 hours. We loaded the alloy specimens with thermal films in a 3.5% NaCl aqueous solution and generated stress (σ) vs ttf curves. On several specimens, we removed the thermal films by CE[12] prior to testing in the corrosive environment.

3. Results and Discussion

For both alloys, the removal of the thermal oxide by the CE technique failed to reduce SCC susceptibility (see Fig. 7), in contrast to the

TABLE III

Composition (wt%) of 7xxx Alloys

Alloy	Zn	Mg	Cu	Cr	Fe	Si	Ti	Mn	Zr	Ni	Al
7075	6.00	2.33	1.62	0.21	0.26	0.12	0.04	0.03	0.01	0.01	Balance
7175	5.62	2.61	1.58	0.20	0.16	0.07	0.03	--	0.04	0.01	Balance
G	4.43	3.73	←		All		<0.01		→		Balance

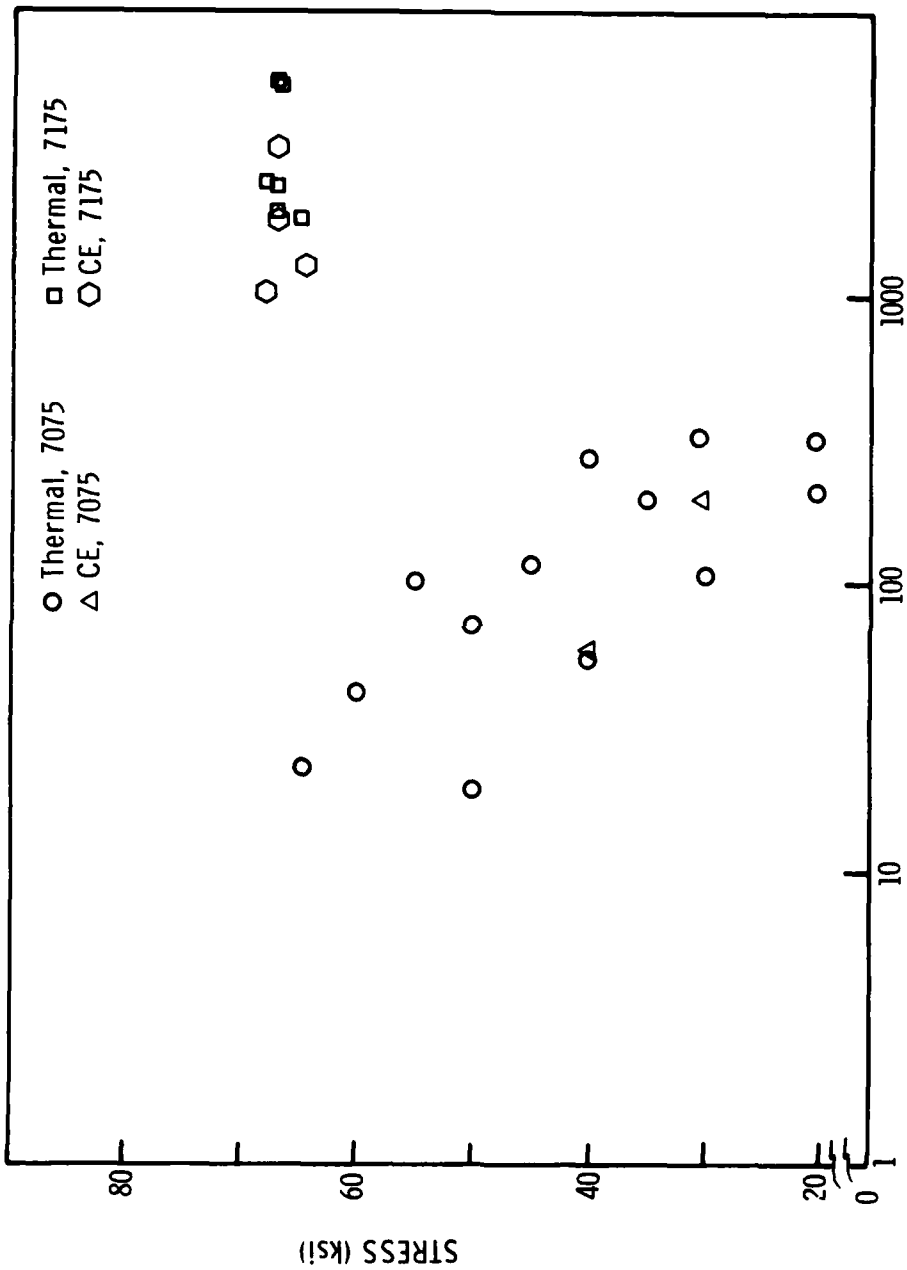

Figure 7. Stress vs time to failure for 7xxx series commercial alloys.

case for the high-purity ternary alloy examined previously.[12] The scatter in the data is substantial, but we found that susceptibility in the 7175 alloy, as expected, was lower than in the 7075 (as shown by the longer ttf).

We believe that the susceptibility of the commercial alloys could not be significantly influenced by the surface oxide because these alloys, unlike our high-purity model alloys, have large constituent particles. A polished cross section containing the SCC fracture profile (Fig. 8) reveals cracking at the impurity constituent particles lying off the main fracture plane. Moreover, the stepped appearance of the SCC fracture profile suggests that a large amount of the cracking occurred near these constituents.

To examine the protective nature of the film above the constituents, we exposed a polished (natural film forms after polishing), unstressed specimen of 7075 to distilled water at room temperature. Attack was found to preferentially occur at the constituent-matrix interface (Fig. 9). We believe the cracking susceptibility produced by the presence of these constituents overrides any benefit resulting from our film control procedures. This explanation is consistent with the lower susceptibility of 7175 compared to 7075 (Fig. 7). Virtually the only difference between these two alloys is the lower impurity content, and consequently, lower constituent particle content of the 7175. In any event, this area does not appear to be fruitful for additional investigation and received no further attention.

7075 SCC

Figure 8. SCC fracture of 7075 showing fracture surface profile and cracking of constituent particles.

Figure 9. SCC initiation at constituent particle in 7075.

C. IDENTIFICATION OF Mg-H COMPLEX BY MICRO-MICRO DIFFRACTION

1. Background

Viswanadham et al. [11] proposed the possibility that a Mg-H complex forms during stress-corrosion crack propagation, based on their observation of free Mg on the grain boundaries of Al-Zn-Mg alloys in susceptible tempers. Tuck,[35] using differential scanning calorimetry (DSC) on Al-Zn-Mg alloys that were exposed to a SCC environment, showed an energy absorption edge at a temperature where decomposition of MgH_2 might be expected. The basic premise is that hydrogen is absorbed into the material during exposure and is bound into a Mg-H complex at the grain boundaries that prevents it from escaping.

Ciaraldi et al. [36] proposed a similar model, but one involving an Al-H complex, and used electron diffraction to identify an Al-H complex.

We attempted to detect these suspected complexes by micro-micro diffraction.

2. Experimental Procedure

We loaded a thin specimen of an Al-Zn-Mg alloy (G) in a corrosive environment (distilled water), removed it, and then prepared it as a thin foil by the electropolishing technique. We placed the foil in a JEOL-100CX scanning transmission electron microscope (STEM), which allows the beam diameter to be reduced to approximately 20 Å. We used the fine beam to generate diffraction patterns from eight very small areas on the foil in the grain boundary region.

3. Results and Discussion

Analysis of the diffraction patterns failed to reveal the presence of Mg-H or Al-H complexes. Diffraction patterns of the hardening

precipitates ($MgZn_2$) and the aluminum matrix were the only ones observed.

The findings suggests several possibilities: 1) a hydride complex is not present, 2) its presence is limited and was not detected, or 3) a hydride formed and decomposed. This last possibility might result from the lack of constraint in the thin foil or from beam heating and radiation damage.

Although the micro-micro diffraction experiments failed to detect the presence of a hydride complex in an Al-Zn-Mg alloy, the interaction of Mg and hydrogen is not precluded. However, the formation of a Mg-H phase still remains speculative.

D. IDENTIFICATION OF Mg-H BY PLASMON-LOSS ENERGY (PLE) MEASUREMENTS

1. Background

In the previous year, we obtained MgH_2 from C.D.S. Tuck, which he used as a standard for his DSC experiment[35] (see Section II.C). We intended to measure the plasmon loss energy (PLE) of Mg in elemental Mg and in MgH_2, and to determine if the values are different. If a difference was shown, we then planned to measure the PLE on specimens that were loaded in a saline environment, removed before fracture, and then fractured under ultrahigh vacuum in the Auger chamber. This experiment was unsuccessful because the MgH_2 supplied by Tuck had been contaminated. AES showed that the contaminant was a mixture of magnesium oxide and hydroxide.

We purchased MgH_2 from Ventron Alpha Corporation, Danvers, Massachusetts and repeated the experiment.

2. Experimental Procedure

The experimental plan was similar to that described above, except that we looked for the Mg-H complex in a cathodically charged Al-4.4wt%Zn-3.7wt%Mg specimen fractured in situ at 10^{-10} torr. In addition, we planned to measure the PLE of Mg in pure magnesium, and in solid solution with Al.

3. Results and Discussion

The high-resolution Auger scan of pure Mg is shown in Fig. 10. The energy of the bulk plasmon is 10.7 eV, which is lower than that of the "free" Mg on the fracture surfaces found in earlier work.[10] This can be explained by noting that an Auger electron released from free Mg on an in-situ fracture surface may lose energy by exciting surface plasmons in the Mg layer or bulk plasmons in the substrate. The bulk

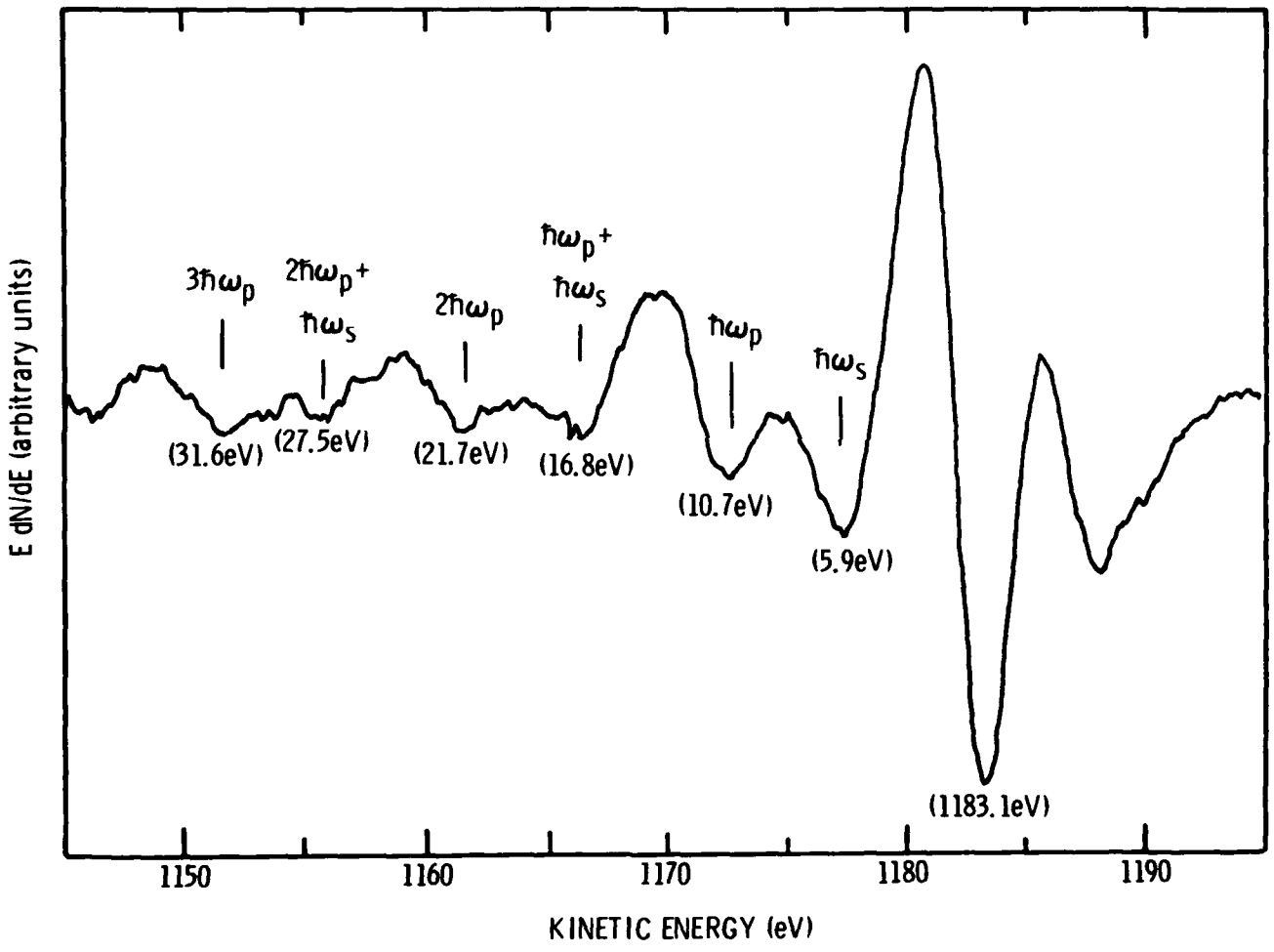

Figure 10. High resolution Auger scan of high purity elemental Mg. Energies in parenthesis denote energy below main Mg peak at 1183.1 eV. Surface plasmons are denoted $\hbar\omega_s$ and bulk plasmons are denoted $\hbar\omega_p$.

PLE of a free Mg surface layer is that of the substrate, most likely an Al-Mg-Zn solid solution in the precipitate free zone (PFZ). The surface PLE (5.9 eV for pure Mg), on the other hand, would be that of the surface layer. It is this measurement that may be used to identify free Mg on grain boundary surfaces.

With the PLE of free Mg well-characterized, we then attempted to measure the PLE of MgH_2 and Mg in solid solution. Unfortunately, AES revealed that the apparent MgH_2 was actually MgO. In case the contamination was only on the surface, we sputtered the samples with inert ions for 1 hour. The composition, however, remained unchanged, indicating a bulk MgO composition or a very thick film. Evidently, MgH_2 is quite reactive and converts to MgO during storage. The experiment was stopped at this stage.

At present, evidence of the suspected Mg-H complex remains elusive.

E. EFFECT OF SOLUTION HEAT-TREATMENT TEMPERATURE (SHT) ON SCC SUSCEPTIBILITY IN Al-Zn-Mg ALLOYS

1. Background

Viswanadham et al.[7] have shown that Mg segregation to the oxide film in Al-Zn-Mg alloys occurs during solution heat treatment, and, moreover, that the extent of this segregation is a sensitive function of SHT. Other studies have shown that SHT can also affect segregation of Mg and Zn in the grain boundary region of Mg- and Zn-containing aluminum alloys.[8-11] For example, Joshi et al.[37] systematically varied SHT for specimens of Al-Zn-Mg-Cu alloy 7075 and aged the specimens to the T6 temper. They fractured the specimens in situ in the Auger chamber at 130°K, which resulted in apparently intergranular fractures, and measured the grain boundary composition by AES. Segregation of Mg, Zn, and Cu were each sensitive functions of SHT over the range of 390 to 530°C, and segregation was minimal for all three elements for specimens solution heat treated at 438°C.

We have shown that SCC susceptibility, in some cases, can be affected by the Mg content of the film,[12,14] and it is well known that grain boundary segregation greatly affects susceptibility in this alloy system.[38,39] Consequently, we believed that variation of SHT might provide a means of controlling segregation and thus reducing SCC susceptibility.

2. Experimental Procedure

We machined tensile specimens of alloy G (Table III), 3 x 0.25 x 0.05 in., with a 1.25-in. gauge length from sheet in the long-transverse direction, and polished them to a 600-grit finish. We also machined and polished notched fracture pins, measuring 1 x 0.125 x 0.05 in., for use in the Auger experiments. Specimens of each type were divided into five

groups and were solution heat treated at 445, 460, 475, 490, or 505°C for 2 hours. All specimens were aged at 150°C for 2 hours to produce peak hardness.[15] The specimens were stored in a dessicator at 0°C until used. The tensile specimens were loaded in a 3.5 wt%NaCl aqueous solution, and stress vs ttf curves were developed.

The fracture pins were fractured in-situ in the Auger chamber at -194°C. This produced fractures that were apparently intergranular, which we characterized by high-resolution AES. We also performed an Auger scan and a depth profile on the surface oxide film of at least one specimen from each group. Thus, the composition of the surface oxide film and the grain boundary could be quantified. We made TEM foils from specimens in each group so that grain boundary precipitate size and spacing could be measured.

3. Results and Discussion

SCC resistance clearly varies with SHT (see Fig. 11): maximum SCC resistance occurs for SHT equal to 460°C, minimum resistance for SHT at 475°C, and only slight differences between the other three SHT groups. The ttf at 75% of the yield stress (ttf_o hereafter) was taken as a convenient parameter for quantifying SCC resistance; this is plotted vs SHT in Fig. 12.

The Auger scans and depth profiles of the surface oxide films did not reveal information that could be clearly correlated with SCC susceptibility. The five depth profiles of the oxide films are in Fig. 13; surface scans are inset. Each oxide film was enriched with Mg. Examination of the oxide morphologies in the STEM also did not reveal differences that could be correlated with SCC susceptibility.

Table IV lists the ratio of Auger peak-to-peak intensity for Mg to Al (Mg:Al) and Zn to Al (Zn:Al) for the fracture specimens. The scatter of these data is quite large, possibly because the fracture path proceeds through the PFZ rather than through the actual grain boundary plane. To verify this conjecture, we pre-exposed an Auger fracture pin

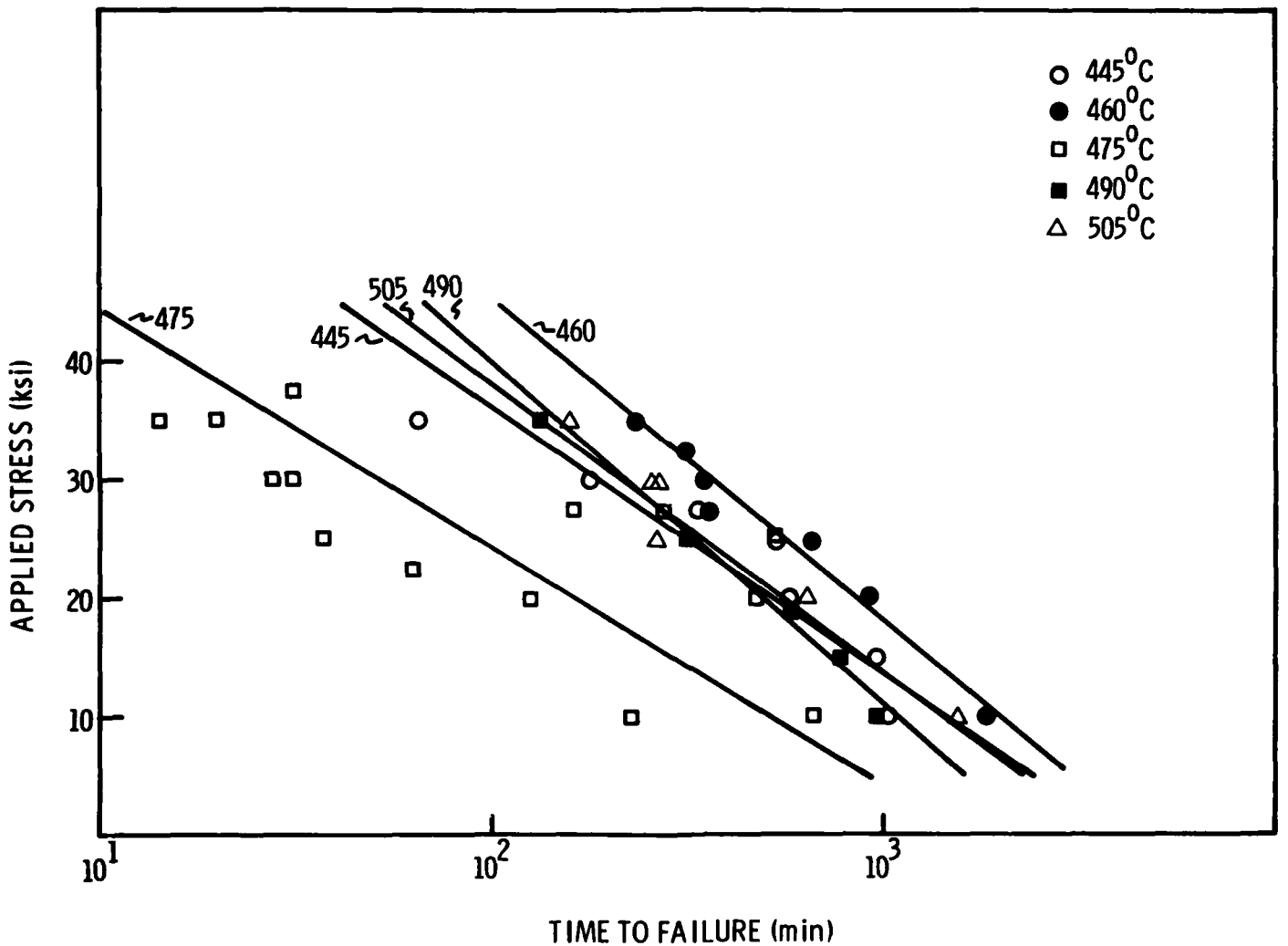

Figure 11. Linear regression of stress vs ttf for the five SHT groups.

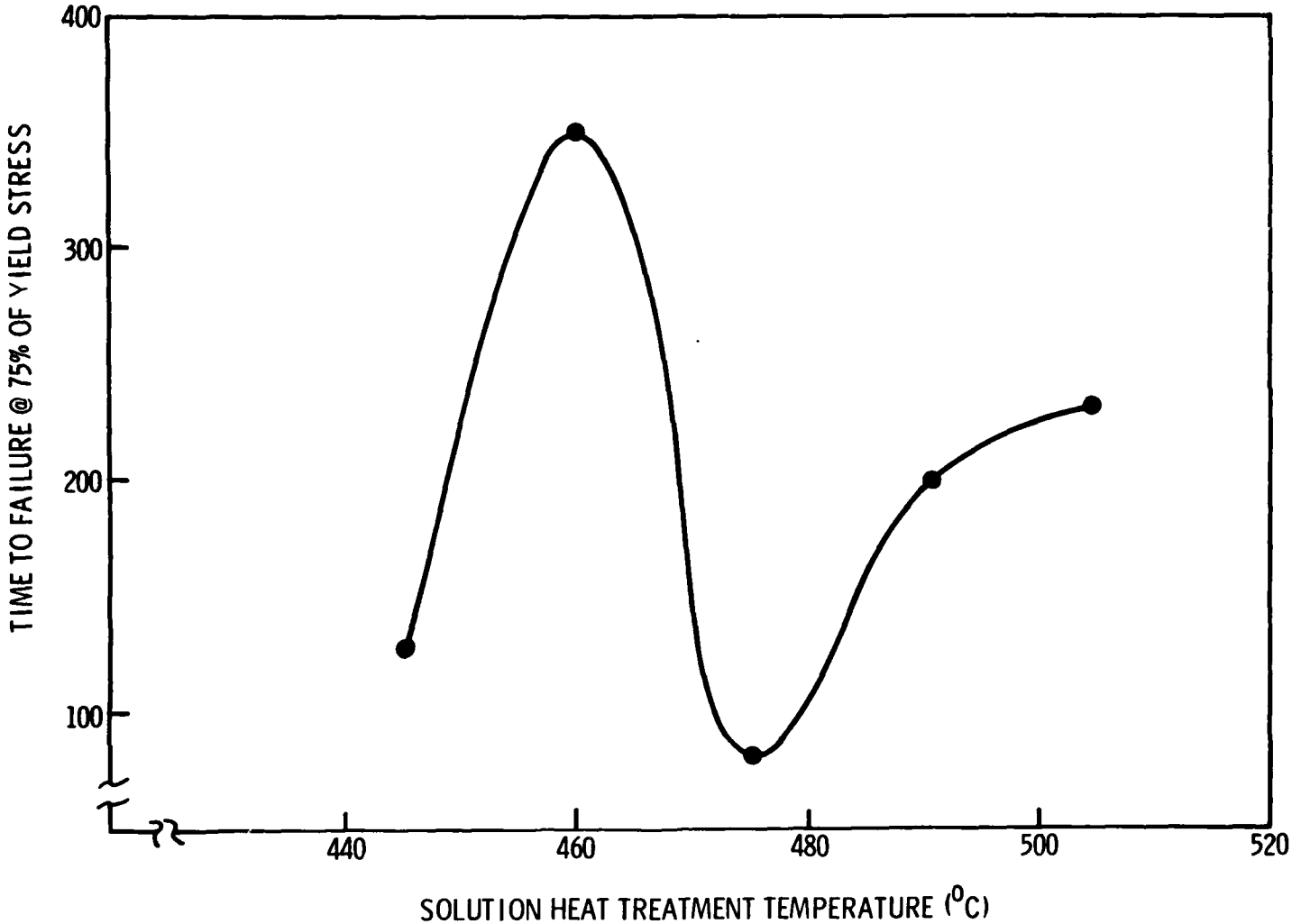

Figure 12. ttf at 75% of the yield stress vs SHT.

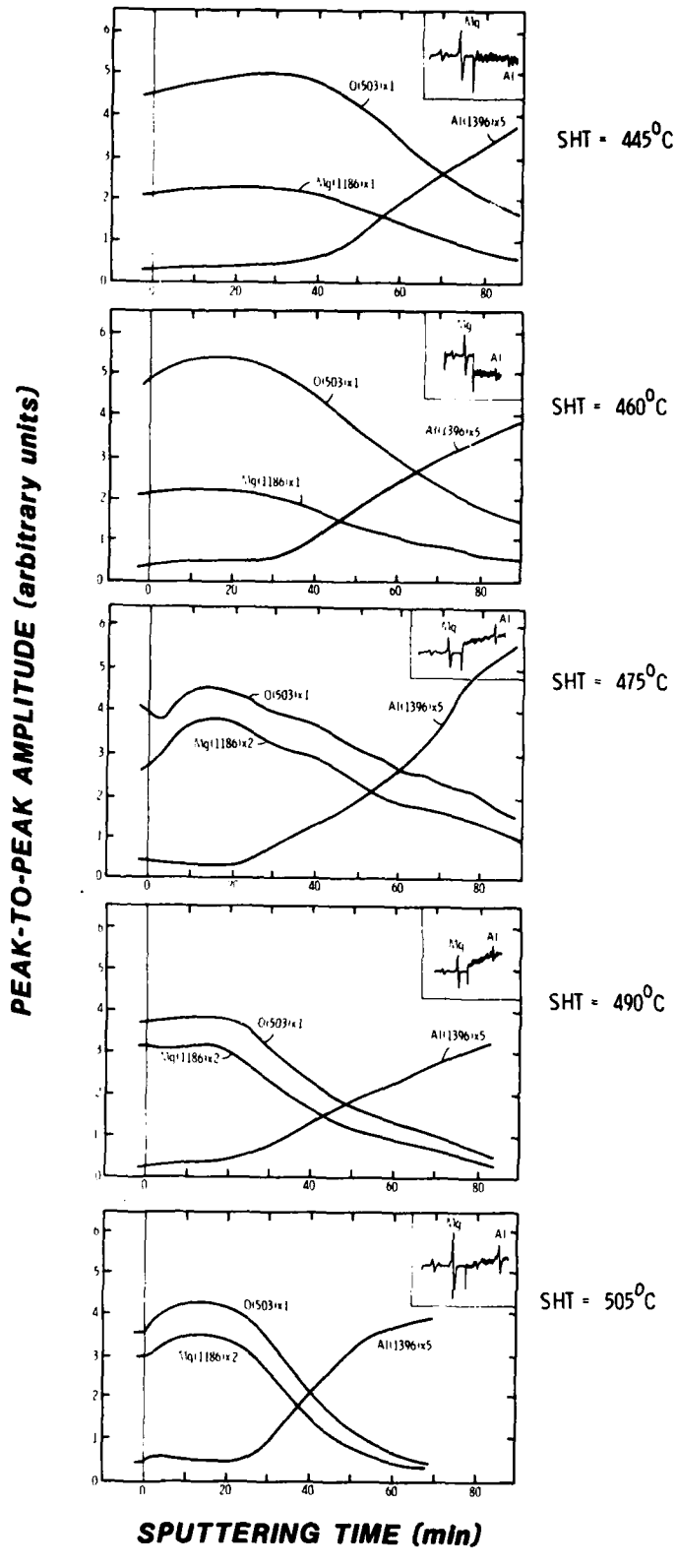

Figure 13. Auger depth profile of thermal oxide films formed at different SHTs. Insert accompanying each profile contains the Auger scan on the surface of each oxide. The number following chemical symbols are the Auger energies and note that the Mg scaling factor is not the same in each figure. Sputtering rate = 30 A/min.

TABLE IV

Peak-to-Peak Intensities from Auger Scans of Intergranular Surfaces Formed by In-Situ Fracture of Al-Zn-Mg Alloy at -194°C

Solution Heat-Treatment Temperature (°C)	Specimen No.	Peak-to-Peak Ratio	
		Mg/Al	Zn/Al
445	1	0.04	0.01
	2	2.83	0.32
	3	1.44	0.06
	4	0.36	0.05
460	1	0.18	0.02
	2	1.74	0.12
	3	0.24	0.04
	4	0.84	0.22
475	1	1.96	<0.01
	2	0.15	0.02
	3	0.14	0.04
490	1	0.13	0.03
	2	0.49	<0.01
	3	0.07	<0.01
	4	0.86	<0.01
505	1	0.07	0.04
	2	0.15	0.04

of commercial Al-Zn-Mg-Cu alloy 7175* to liquid Ga at 50°C for 2 hours. Ga is known to penetrate the grain boundaries of aluminum alloys and is believed to induce fracture along the grain boundary plane.[40,41] This specimen, and another 7175 specimen that was not pre-exposed to Ga, were fractured at -194°C in the Auger chamber, and high-resolution scans were performed. Mg:Zn for the nonexposed specimen was 0.05, but the value for the pre-exposed specimen was 1.7. This result suggests that fracture in the nonexposed specimen propagated in part along the PFZ (which was probably solute depleted), while the fracture path in the Ga pre-exposed specimens was along the actual boundary plane. The zinc-to-aluminum peak-to-peak ratio (Zn:Al) could be measured only with limited accuracy because two Ga Auger peaks at 985 and 1000 eV obscure the Zn peak at 994 eV.

The shape of the Auger transitions and the energies of plasmon satellite peaks can provide information on the binding state of Mg in the oxide and the grain boundary. The shapes of the transitions for Mg on the oxides in this study clearly indicate that the Mg exists essentially as MgO. There is no evidence of elemental Mg in the film (which might trap hydrogen and aid in embrittlement). Table V gives the plasmon-loss energies of the Mg and Zn peaks measured on the "grain boundary" fracture planes. The interpretation of these data is not straightforward. An Auger electron escaping from a Mg atom may lose some of its energy by exciting plasmon waves in the free-electron cloud in the material from which it escapes. In this case, the material could be: 1) elemental Mg on the grain boundary, 2) $MgZn_2$ grain-boundary precipitates, or 3) a dilute solid solution of Mg and Zn in aluminum (the PFZ). To complicate matters further, the plasmon from Mg may be from the surface or the bulk. At present, we do not know the PLE values for all of these possibilities with certainty. The plasmon satellite peaks from the various alloy G specimens were often broad, suggesting that the values we measured for the PLE for Mg and Zn may contain contributions from several of the kinds of plasmons noted.

* At the time of this experiment, only 7175 Auger pins were available. Specimens of alloy G broke shortly after wetting by Ga, and so could not be loaded into the Auger chamber. We will test additional specimens pre-exposed to Ga in the near future.

TABLE V

Plasmon Loss Energies (PLE) of Mg, Zn, and Al on Intergranular Surfaces Formed by In Situ Fractures of Al-Zn-Mg Alloy at -194°C

Solution Heat-Treatment Temperature (°C)	PLE (eV)		
	Mg	Zn	Al
445	14.8	13.9	15.2
460	14.0	13.4	14.6
475	13.7	14.6	15.0
490	13.2	12.8	15.2
505	13.3	11.8	15.2

The PLE data fail to explain the observed differences in susceptibility, most probably because fracture does not proceed along the actual grain boundary plane. Therefore, random contributions to the PLE from regions off the grain boundary plane may have been introduced. Nevertheless, the PLE values for Mg and Zn generally decrease with SHT, suggesting that increasing amounts of solute lie in the $MgZn_2$ precipitates.[10] This may be explained by the greater amount of quenched-in vacancies occurring with increasing SHT, which increases solute mobility during aging, leading to increased segregation in $MgZn_2$ precipitates.

We are repeating the Auger fracture tests on specimens from the five SHT groups that were pre-exposed to Ga. The gallium pre-exposure should ensure that the fracture exposes the actual grain boundary plane, thereby enabling accurate measurement of grain boundary segregation. In addition, we are in the process of examining TEM foils made from the specimens in the five SHT groups to determine differences in grain-boundary precipitate size and spacing that might explain the differences in SCC susceptibility.

At present, we believe that the compositions of the oxide films are sufficiently similar that they do not account for the differences in susceptibility. The segregation and microstructural features of the grain boundary that may explain the differences in susceptibility have not yet been identified.

REFERENCES

1. A.J. Sedriks, J.A.S. Green, D.L. Novak: "Corrosion Processes and Solution Chemistry Within Stress Corrosion Cracks in Aluminum Alloys," in Localized Corrosion NACE-3, NACE, Houston, 1974, pp. 569-575.

2. E.N. Pugh, J.A.S. Green, and A.J. Sedriks: "Current Understanding of Stress Corrosion Phenomena," in Proc. Int. Conf. on Interfaces, August 1969, pp. 237-256. Also RIAS Tech. Rept. 69-3, Baltimore, MD.

3. A.J. Sedriks, J.A.S. Green, and D.L. Novak: "On the Chemistry of the Solution at Tips of Stress Corrosion Cracks in Al Alloys," Corrosion NACE, 1971, vol. 27, no. 5, p. 198.

4. J.A.S. Green and H.W. Hayden: "Influence of Two Modes of Loading on the Stress Corrosion Susceptibility of Ti-8Al-1Mo-1V Alloy in Various Chloride-Containing Environments," in Hydrogen in Metals, I.M. Bernstein and A.W. Thompson, eds., ASM, Metals Park, OH, 1974, pp. 235-244.

5. J.A.S. Green, H.W. Hayden, and W.G. Montague: "The Influence of Loading Mode on the Stress Corrosion Susceptibility of Various Alloy/Environment Systems," in Proc. Conf. on Effects of Hydrogen on Behavior of Materials, A.W. Thompson and I.M. Bernstein, eds., AIME, Philadelphia, PA, 1976, p. 200.

6. T.S. Sun, J.M. Chen, R.K. Viswanadham, J.A.S. Green: "Surface Activities of Mg in Al Alloys" J. Vac. Sci. Technol., vol. 16, no. 2, March/April 1979.

7. R.K. Viswanadham, T.S. Sun, and J.A.S. Green: "Influence of Moisture Exposure on the Composition of Oxides on Al-Zn-Mg Alloy: An Auger Electron Spectroscopy Study," Corrosion, 1980, vol. 36, no. 6, p. 275.

8. J.A.S. Green and W.G. Montague: "Observations on the Stress Corrosion Cracking of an Al-5%Zn-2.5%Mg Ternary and Various Quarternary Alloys," Corrosion, 1975, vol. 31, no. 6, pp. 209-213.

9. J.A.S. Green, R.K. Viswanadham, T.S. Sun, and W.G. Montague: "Grain Boundary Segregation and Stress Corrosion Cracking of Aluminum Alloys," in Corrosion/77, Proc. Int. Corrosion Forum, Paper 17, Natl. Assoc. Corros. Eng., San Francisco, CA, 1977, p. 17/1.

10. T.S. Sun, J.M. Chen, R.K. Viswanadham, and J.A.S. Green: "Plasmon-Loss Satellites in Auger Spectra of Alloy Surfaces," Appl. Phys. Lett., 1977, vol. 31, no. 9, pp. 580-582.

11. R.K. Viswanadham, T.S. Sun, and J.A.S. Green: "Grain Boundary Segregation in Al-Zn-Mg Alloys -- Implications to Stress Corrosion Cracking," Metall. Trans. A, 1980, vol. 11A, p. 85.

12. J.R. Pickens, D. Venables, and J.A.S. Green: "The Delayed Fracture of Aluminum Alloys," Report for ONR contract N00014-74-C-0277, P00006, Martin Marietta Laboratories, May 1980.

13. J.R. Pickens, D. Venables, and J.A.S. Green: "Effect of Zn/Mg Ratio on Stress-Corrosion Susceptibility of Al-Zn-Mg Alloys," Submitted for publication in Met. Trans.

14. J.R. Pickens, D. Venables, and J.A.S. Green: "Improved SCC Resistance of Al-Zn-Mg Alloys by Control of Mg Content in the Bulk Metal and In the Oxide Film," in Hydrogen Effects in Metals, Proc. 3rd Int. Conf. on the Effect of Hydrogen on the Behavior of Materials, Jackson Lake, WY, August 26-29, 1980, pp. 513-523.

15. J.R. Pickens, D. Venables, and J.A.S. Green: "The Delayed Fracture of Aluminum Alloys," End-of-year report on ONR contract N00014-74-C-0277, Martin Marietta Laboratories, Jan. 1981.

16. H.W. Hayden and S. Floreen: "Effect of Various Modes of Loading on the Stress Corrosion Cracking of Maraging Steel," Corrosion NACE, 1971, vol. 27, no. 10, pp. 429-433.

17. J.C.M. Li, R.A. Oriani, and L.S. Darken: "The Thermodynamics of Stress Solids," Z. Phys. Chem. Neue Folge, 1966, vol. 49, pp. 271-290.

18. N. Pugh: Presentation at the Conference Environmental Degradation of Engineering Materials, Sept. 21-23, 1981, Virginia Polytechnic Institute, Blacksburg, VA.

19. J.A.S. Green, H.D. Mengelberg, and H.T. Yolken: "An Ellipsometric Study of Oxide Growth Kinetics for Copper and Alpha-Brasses in Aqueous Ammonia," J. Electrochem. Soc., 1970, vol. 117, pp. 433-437.

20. D.O. Sprowls and R.H. Brown: "Stress Corrosion Mechanism for Aluminum Alloys," in Proc. Conf. on Fundamental Aspects of Stress Corrosion Cracking, R.W. Staehle, A.J. Forty, D. Van Rooyer, eds., Ohio State University Press, Columbus, 1969, pp. 466-506, discussion pp. 506-512.

21. D.O. Sprowls, M.B. Shumaker, J.W. Coursen, and J.D. Walsh: "Evaluations of Stress Corrosion Cracking Susceptibility Using Fracture Mechanics Techniques," Final Report, Part I (period July 1, 1968 - August 31, 1972), May 31, 1973, Contract No. NAS 8-21487, for George C. Marshall Space Flight Center.

22. D.O. Sprowls: Alcoa Technical Center, Pittsburgh, PA, private communication to J.R. Pickens, Martin Marietta Laboratories, 1980.

23. 1980 Annual Book of ASTM Standards, part 10, ASTM E399-789, American Society for Testing and Materials, 1966, pp. 580-601.

24. W.F. Brown and J.E. Strawley: ASTM STP 410, 129 pp., American Society for Testing and Materials, 1966.

25. H. Tada, P. Paris, and G. Irwin: The Stress Analysis of Cracks Handbook, Del Research Corp., Hellertown, PA, 1973.

26. M.P. Rozanov and V.I. Smirnov: "Method of Experimental Determination of K_{IIIC}," Ind. Lab., 1979, vol. 45, no. 7, p. 830.

27. T. Ohnishi, K. Higashi, N. Inoue, and Y. Nakatani: "Effects of Alloying Elements on Hydrogen Embrittlement of Al-8%Mg Alloy," J. Jpn. Inst. Light Met., 1980, vol. 30, no. 5, pp. 263-270.

28. T. Ohnishi, K. Higashi, and Y. Nakatani: J. Jpn. Inst. Met. Sendai, 1981, vol. 45, no. 4, pp. 373-378.

29. K. Higashi, T. Ohnishi, Y. Nakatari, and K. Okabayashi: "Formation and Disappearance of Pre-Existing Embrittled Zone Ahead of Stress Corrosion Cracks," J. Jpn. Inst. Light Met., 1981, vol. 31, no. 6, pp. 386-392.

30. T. Ohnishi and K. Higashi: "Effects of Hydrogen on the Stress Corrosion Cracking of Al-8%Mg," Aluminium, 1981, no. 8, pp. 558-559.

31. P.R. Swann: Discussion in Hydrogen in Metals, I.M. Bernstein and A.W. Thompson, eds., ASM, Metals Park, OH, 1974, p. 274.

32. M.V. Hyatt and M.O. Speidel: Chapter 4 of Stress-Corrosion Cracking in High Strength Steels and in Titanium and Aluminum Alloys, B.F. Brown, ed., Nav. Res. Lab., 1972, pp. 147-244.

33. D. Broek: Elementary Engineering Fracture Mechanics, Noordhoff International Publishers, Leyden, Netherlands, 1974.

34. P.F. Thomson and N.M. Burman: "Edge Cracking in Hot-Rolled Al-Mg Alloys," Mater. Sci. Eng., 1980, vol. 45, pp. 95-107.

35. C.D.S. Tuck: "Evidence for the Formation of Magnesium Hydride on the Grain Boudaries of Al-Mg and Al-Zn-Mg Alloys During Their Exposure to Water Vapour," in Hydrogen Effects in Metals, Proc. 3rd Int. Conf. on the Effect of Hydrogen on the Behavior of Materials, Jackson Lake, WY, August 26-29, 1980, pp. 503-511.

36. S.W. Ciaraldi, J.L. Nelson, R.A. Yeske, and E.N. Pugh: "Studies of Hydrogen Embrittlement and Stress-Corrosion Cracking in an Aluminum-Zinc-Magnesium Alloy," in Hydrogen Effects in Metals, Proc. 3rd Int. Conf. on the Effect of Hydrogen on the Behavior of Materials, Jackson Lake, WY, August 26-29, 1980, pp. 437-447.

37. A. Joshi, C.R. Shastry, and M. Levy: "Effect of Heat Treatment on Solute Concentration at Grain Boundaries in 7075 Aluminum Alloy," Met. Trans. A, 1981, vol. 12A, pp. 1081-1088.

38. C.J. Peel and P. Poole: "Stress Corrosion Cracking of High Strength Al-Zn-Mg-Cu Alloys - Solute Depletion at Grain Boundaries," Royal Aircraft Establishment Tech. Report 77148, 28 Sept 1977.

39. P. Doig and J.W. Eddington: "Stress Corrosion Susceptibility of As-quenched Al-5.9wt%Zn-3.2wt%Mg Alloys," Br. Corros. J., 1974, vol. 9, no. 4, pp. 220-222.

40. W.R. Goggin and J.W. Moberly: "Direct Observation of the Liquid Metal Embrittlement of Aluminum by Gallium," Trans. Am. Soc. Met., 1966, vol. 59, pp. 315-323.

41. A.R.C. Westwood, C.M. Preece, and M.H. Kamdar: "Adsorption-Induced Brittle Fracture in Liquid Metal Environments," Martin Marietta Laboratories, Tech. Report 67-8c, May 1967, on Contract DA-001-AMC-1109(x).